AI for Nuclear Medicine in Oncology

Mehdi Maghsudi, MD

Department of Nuclear Medicine & Molecular Imaging

Rajaie Cardiovascular, Medical & Research Center

SHAHEED RAJAIE
Cardiovascular Medical & Research Institute

دپارتمان پزشکی هسته‌ای و تصویربرداری مولکولی (PET/CT)
Department of Nuclear Medicine and Molecular Imaging

Iran University of Medical Sciences

Introduction

- **Nuclear Medicine** in **Oncology**:

- **Conventional** Imaging : **Planar**, **SPECT**, **SPECT/CT**

- **PET** Imaging : **PET/CT**, **PET/MR**

- **Therapy** : **Theragnostic**

PET/CT

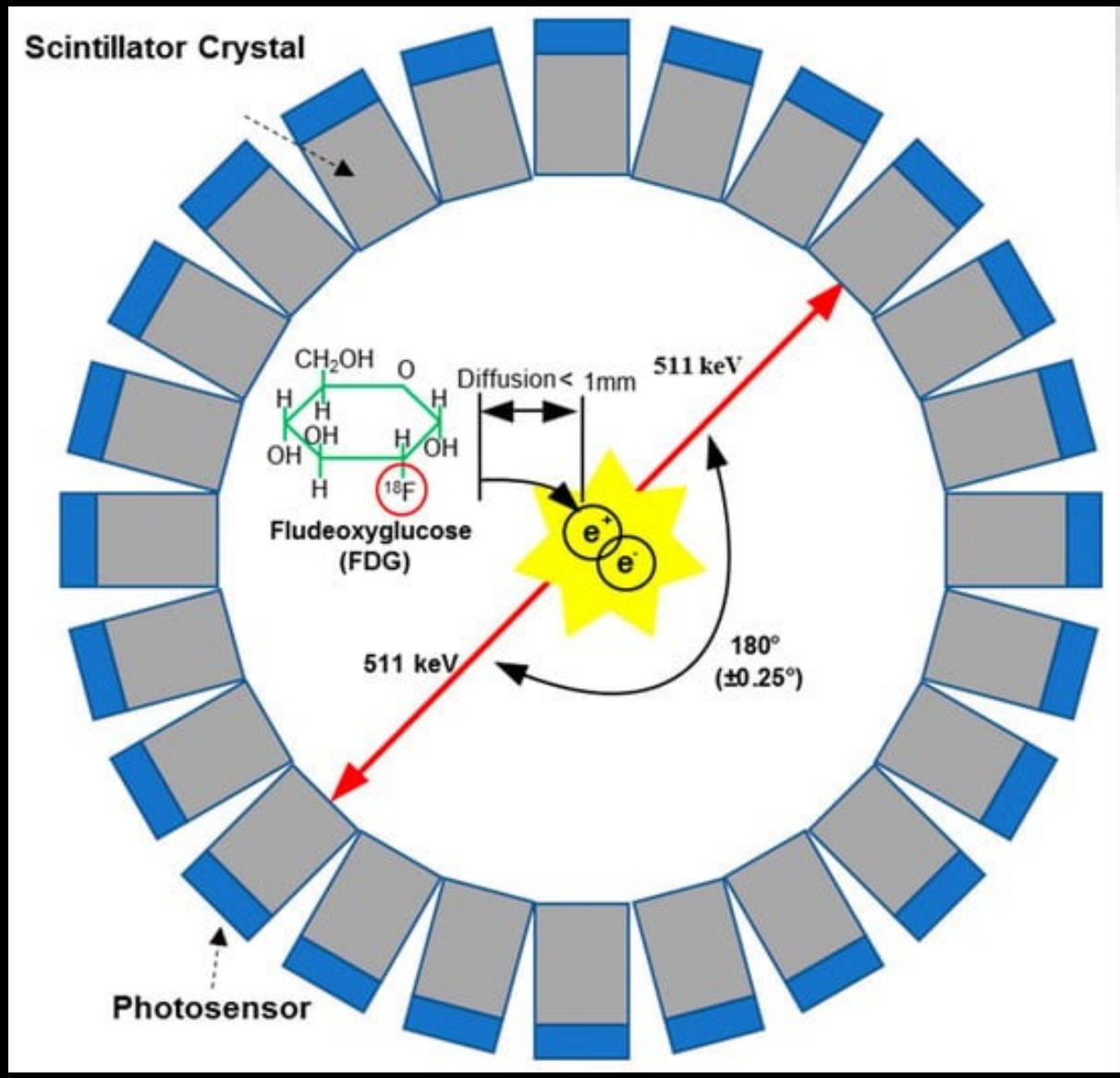
Scintillator Crystal
CH2OH
O
H
H
H
OH
H
OH
OH
H
18F
Fludeoxyglucose
(FDG)
Diffusion < 1mm
511 keV
e+
e-
180°
(±0.25°)
511 keV
Photosensor

Outline

- CADe/ Lesion Segmentation
- CADx
- Image Quality
- Survival Prediction
- Virtual Image

CADe

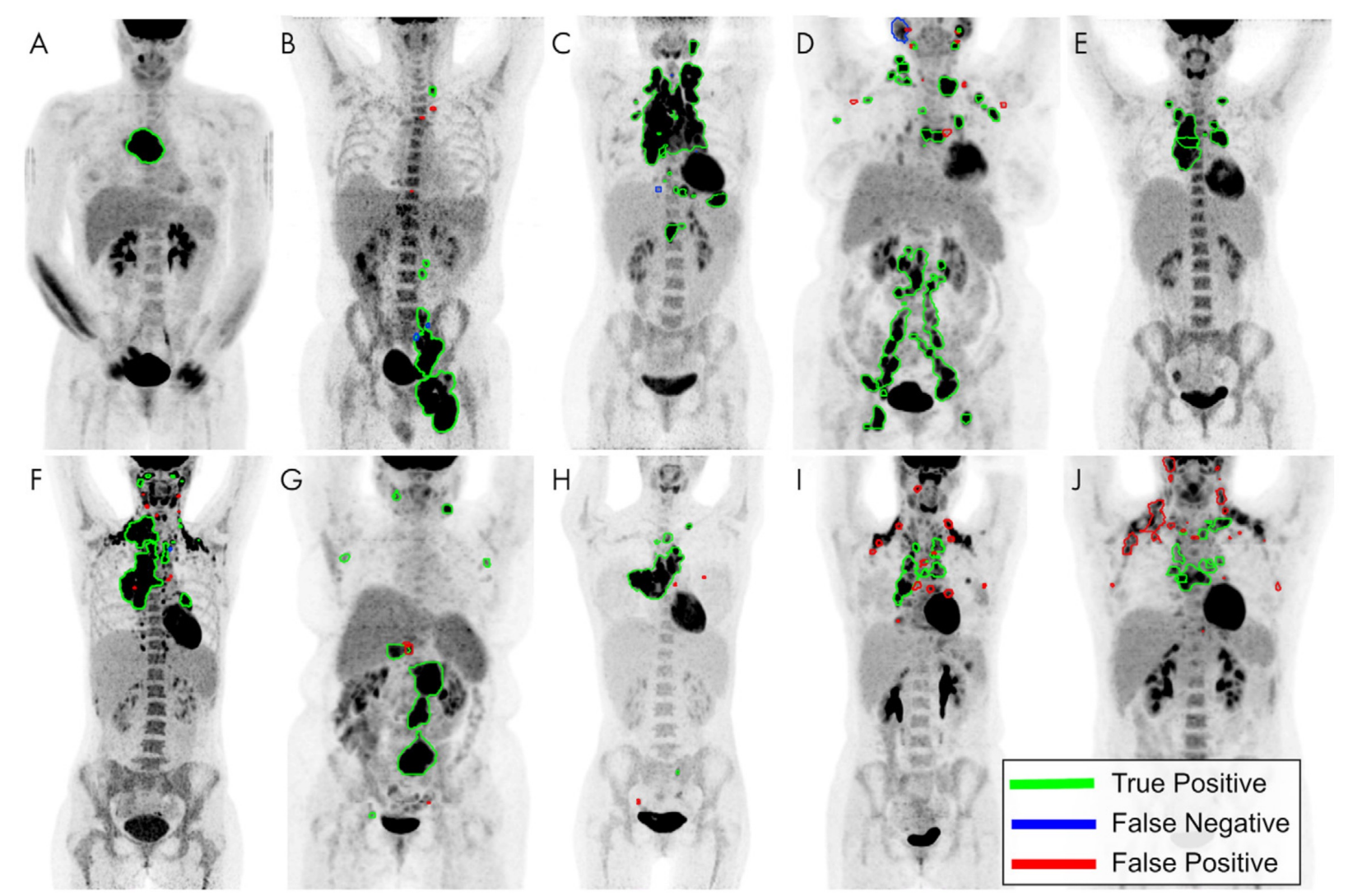

Convolutional Neural Networks for Automated PET/CT Detection of Diseased Lymph Node Burden in Patients with Lymphoma
Amy J. Weisman, Minnie W. Kieler, Scott B. Perlman, Martin Hutchings, Robert Jeraj, Lale Kostakoglu, and Tyler J. Bradshaw
Radiology: Artificial Intelligence 2020 2:5

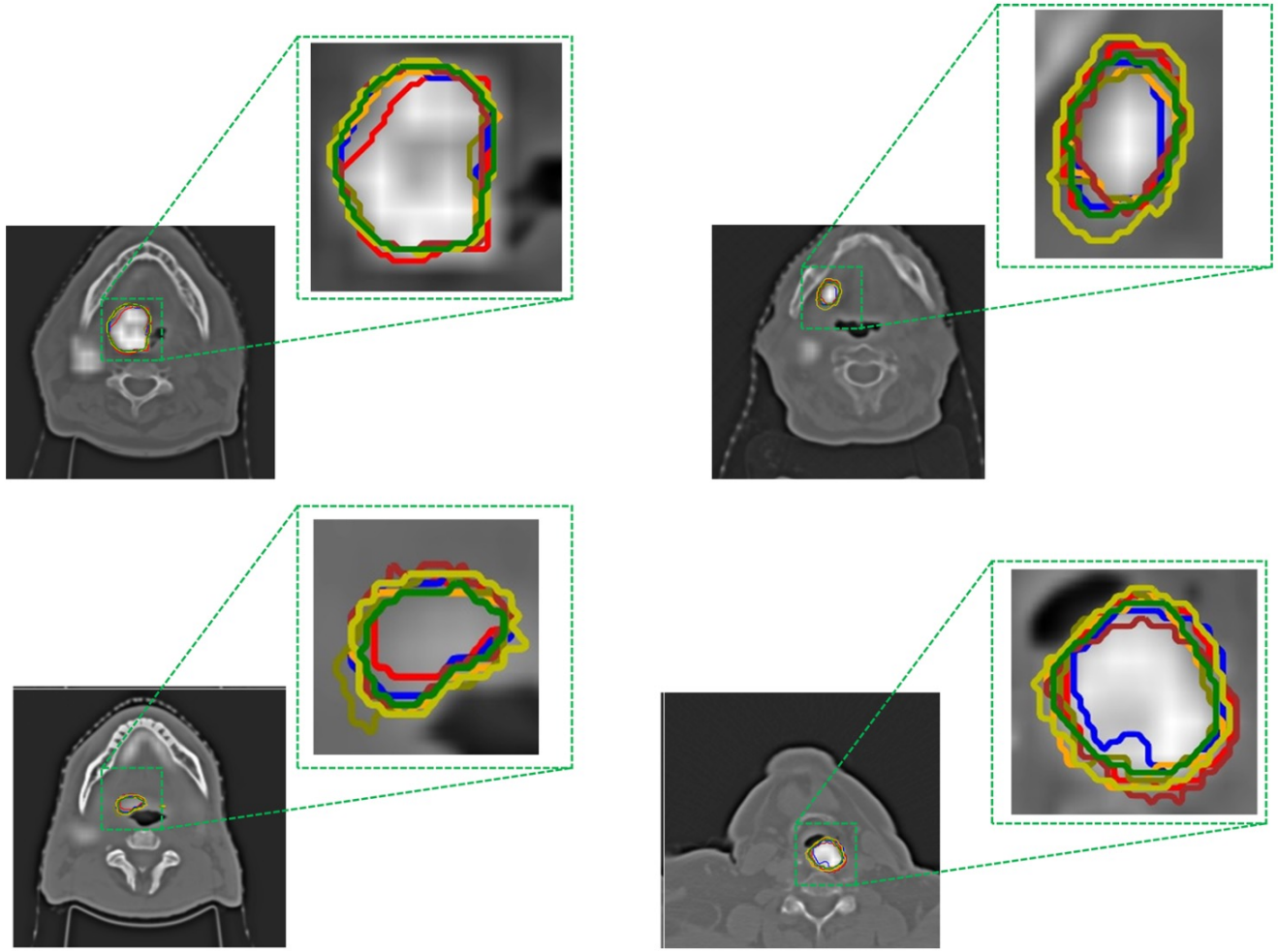

FIGURE 3 Visualization of segmentation output of representative clinical studies on transaxial slices with their corresponding zoomed version. Manual: Red; PET: Green, MDLatLRRR: Blue, Fusion_Ils: orange, Fusion_DLs: Olive, FusionNLs: Brown, Staple All: Yellow, Majority All: Cyan.

Shiri I, et al. Information fusion for fully automated segmentation of head and neck tumors from PET and CT images. Med Phys. 2023 Jul 20. doi: 10.1002/mp.16615. Epub ahead of print. PMID: 37475591.

CADx

Artificial intelligence-based analysis of whole-body bone scintigraphy: The quest for the optimal deep learning algorithm and comparison with human observer performance

Ghasem Hajianfar [a], Maziar Sabouri [b,c], Yazdan Salimi [a], Mehdi Amini [a], Soroush Bagheri [c], Elnaz Jenabi [d], Sepideh Hekmat [e], Mehdi Maghsudi [c], Zahra Mansouri [a], Maziar Khateri [f], Mohammad Hosein Jamshidi [g], Esmail Jafari [h], Ahmad Bitarafan Rajabi [c], Majid Assadi [h], Mehrdad Oveisi [i], Isaac Shiri [a], Habib Zaidi [a,j,k,l,*]

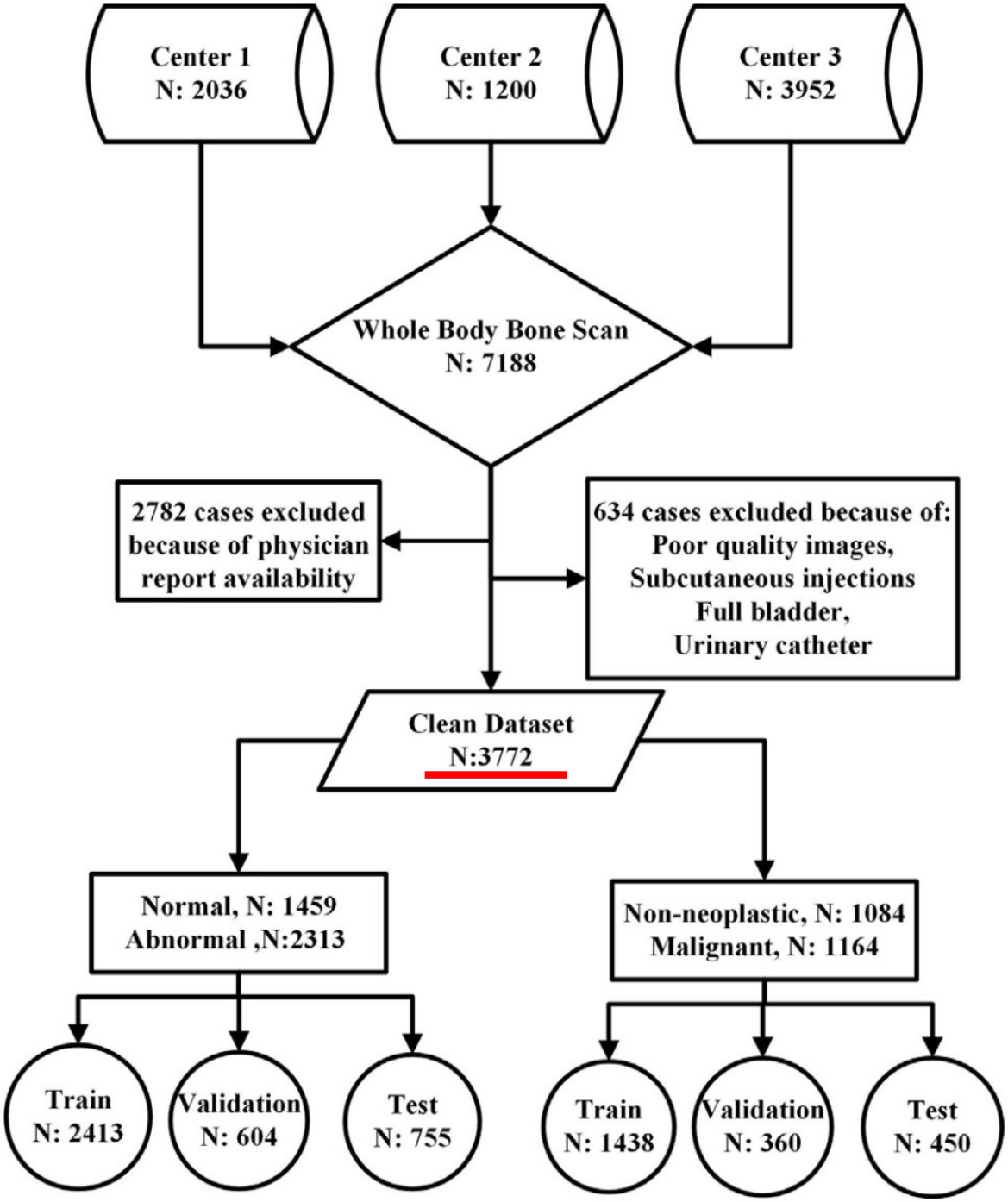

Figure 1. Flowchart of inclusion and exclusion criteria.

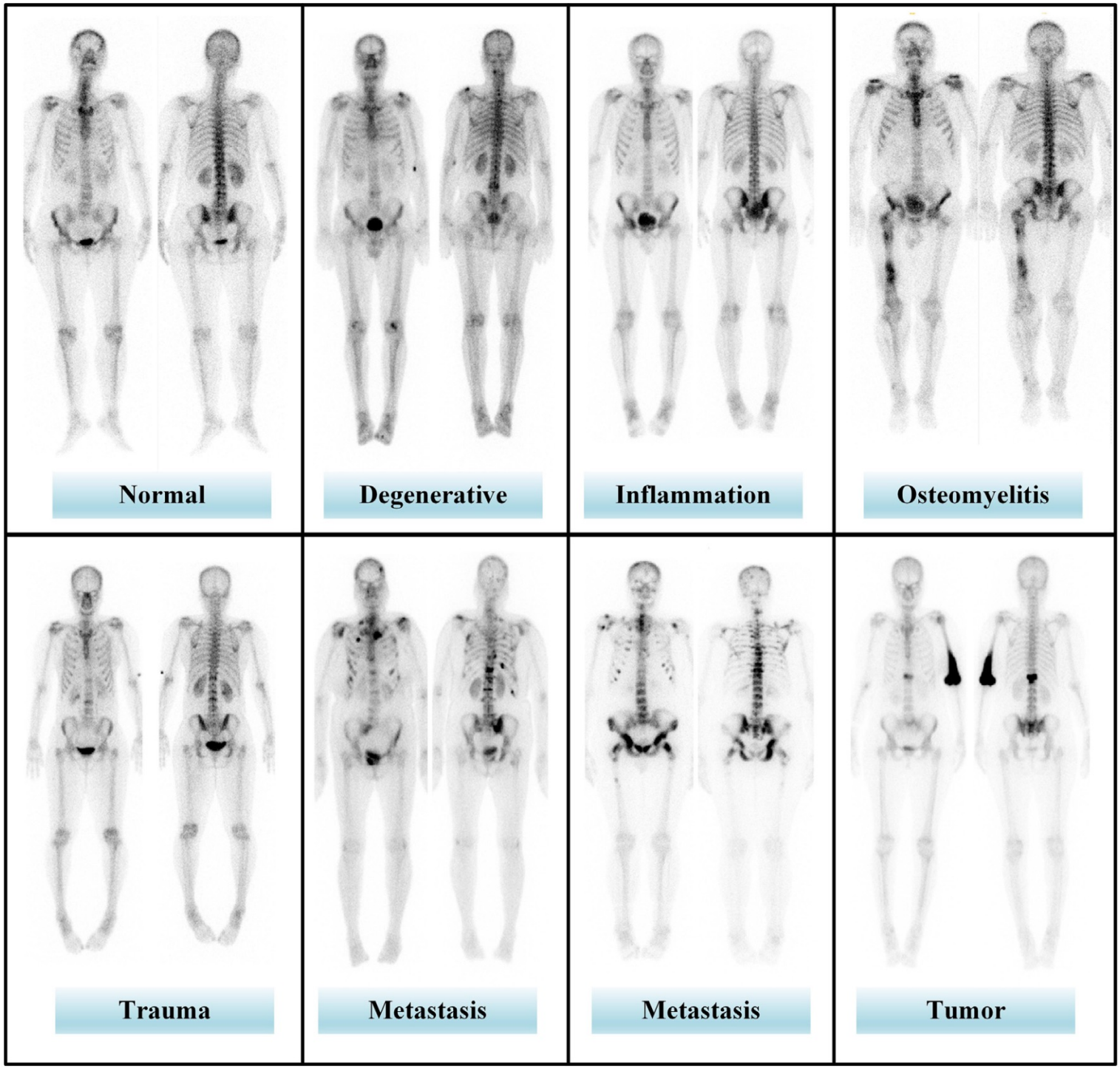

Figure 2. An instance of normal and pathological cases according to nuclear medicine physicians' reports.

Table 6
Comparison of the performance of three nuclear medicine physicians (NMP) vs. artificial intelligence (AI) models* with the highest AUC in each analysis.

Analysis		TN	TP	FN	FP	ACC	AUC	SEN	SPE	Time
Analysis 1 (Normal vs. Abnormal)	NMP1	111	430	166	48	0.72	0.65	0.72	0.70	180 min
	NMP2	97	445	33	180	0.72	0.64	0.93	0.35	110 min
	NMP3	77	436	200	42	0.68	0.60	0.69	0.65	210 min
	AI	195	348	130	82	0.72	0.72	0.73	0.70	28 sec
Analysis 2 (Malignant Vs. Non-neoplastic)	NMP1	198	135	23	94	0.74	0.74	0.85	0.68	112 min
	NMP2	137	180	49	84	0.70	0.70	0.79	0.62	120 min
	NMP3	189	156	32	73	0.77	0.77	0.83	0.72	180 min
	AI	195	126	103	26	0.71	0.72	0.55	0.88	25 sec

* TN: true negative, TP: true positive, FN: false negative, FP: false positive, ACC: Accuracy, AUC: area under the ROC curve, SEN: sensitivity, SPE: specificity. The AI model in analysis 1 and 2 was DenseNet121_AA and InceptionResNetV2_SPP, respectively.

Quality

European Journal of Nuclear Medicine and Molecular Imaging
https://doi.org/10.1007/s00259-023-06418-7

ORIGINAL ARTICLE

Check for updates

Differential privacy preserved federated transfer learning for multi-institutional ^{68}Ga-PET image artefact detection and disentanglement

Isaac Shiri[1,2] · Yazdan Salimi[1] · Mehdi Maghsudi[3] · Elnaz Jenabi[4] · Sara Harsini[5] · Behrooz Razeghi[6] · Shayan Mostafaei[7,8] · Ghasem Hajianfar[1] · Amirhossein Sanaat[1] · Esmail Jafari[9] · Rezvan Samimi[10] · Maziar Khateri[11] · Peyman Sheikhzadeh[12] · Parham Geramifar[4] · Habibollah Dadgar[13] · Ahmad Bitrafan Rajabi[3,14] · Majid Assadi[9] · François Bénard[5,15] · Alireza Vafaei Sadr[16,17] · Slava Voloshynovskiy[6] · Ismini Mainta[1] · Carlos Uribe[15,18,19] · Arman Rahmim[15,19,20] · Habib Zaidi[1,21,22,23]

Received: 14 April 2023 / Accepted: 24 August 2023
© The Author(s) 2023

Table 1 Image acquisition and reconstruction settings in 8 different imaging centres

Centre	No	Clean	Train	Test	Scanner	Reconstruction	Tracers	Matrix size
Centre 1	70	16	12	4	Siemens Horizon	PSF + TOF + 3D-OSEM	^{68}Ga-PSMA	180 × 180
Centre 2	315	71	56	15	Siemens Biograph 6	3D-OSEM	^{68}Ga-PSMA	168 × 168
Centre 3	97	49	39	10	Siemens mCT	PSF + TOF + 3D-OSEM	^{68}Ga-PSMA	256 × 256
Centre 4	97	49	39	10	Siemens Vision	PSF + TOF + 3D-OSEM	^{68}Ga-PSMA	440 × 440
Centre 5	261	51	40	11	Siemens Biograph 6	PSF + 3D-OSEM	^{68}Ga-PSMA	168 × 168
Centre 6	295	57	45	12	Siemens mCT	3D-OSEM	^{68}Ga-PSMA	200 × 200
Centre 7	183	89	71	18	GE Discovery 690	3D-OSEM	^{68}Ga-DOTA-TATE	192 × 192
Centre 8	95	39	31	8	GE Discovery IQ	3D-OSEM	^{68}Ga-PSMA	192 × 192
Total	1413	421	333	88	-	-	–	-

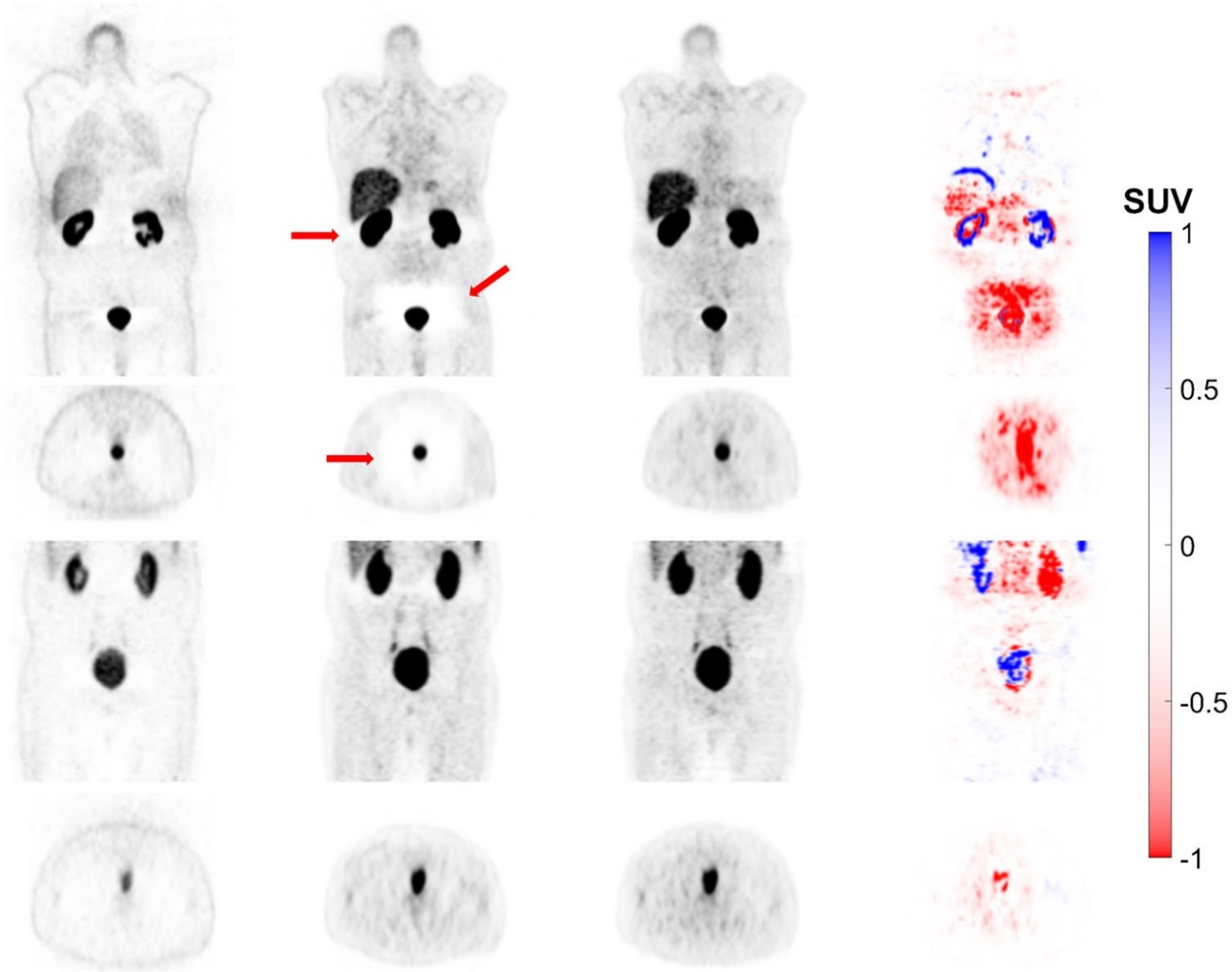

Fig. 5 Coronal and axial views showing from left to right: non-ASC, CT-ASC, FTL-ASC and the difference images of CT-ASC and FTL-ASC. The top panel shows the initial scan, whereas the bottom panel depicts the repeated scan in the artefacted region (depicted by the arrows). In the repeated CT-ASC scan, this artefact was removed from the images. FTL-ASC produced high-quality artefact-free images in both scans

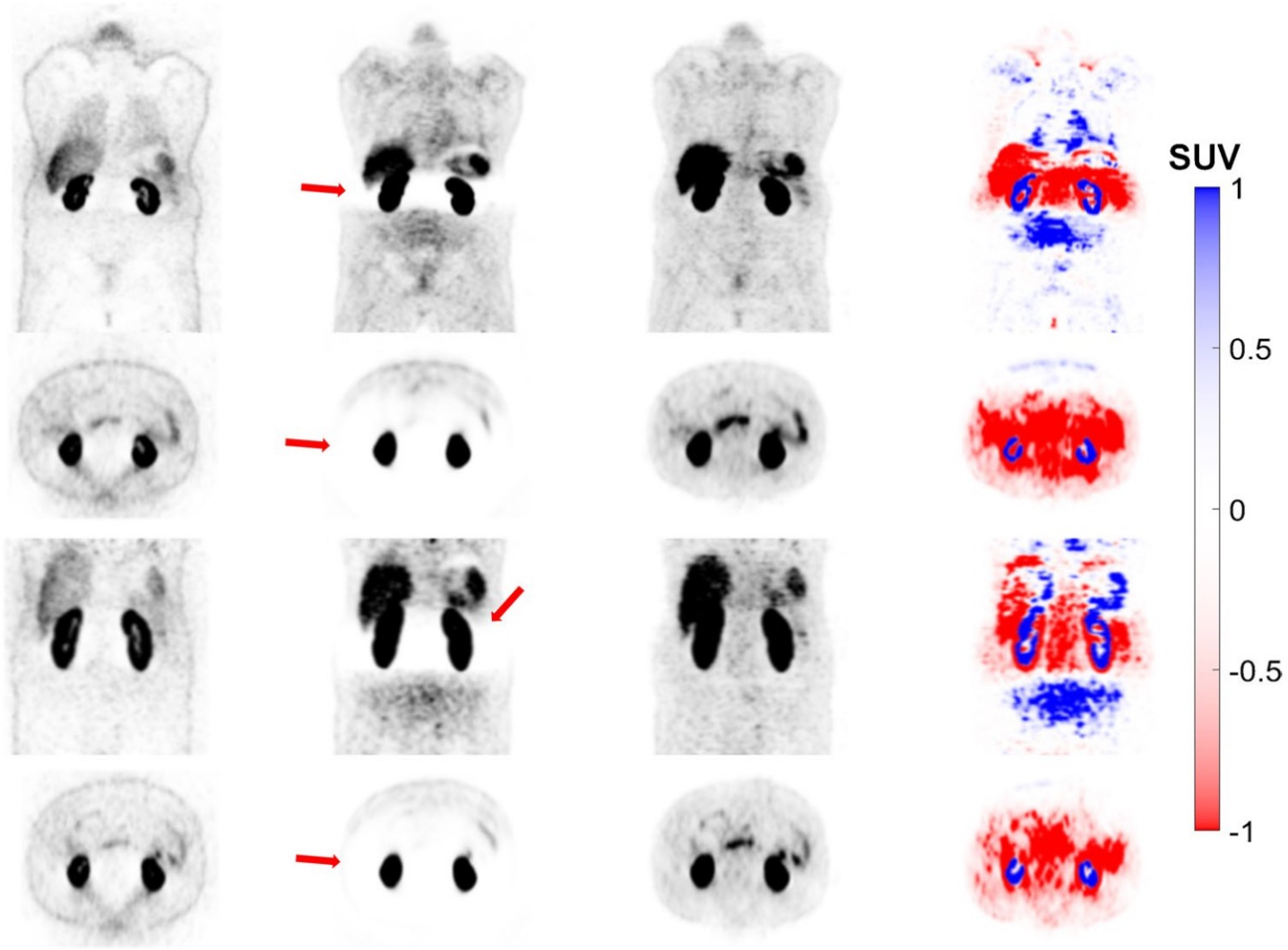

Fig. 6 Coronal and axial views showing from left to right: non-ASC, CT-ASC, FTL-ASC and the difference images of CT-ASC and FTL-ASC. The top panel shows the initial scan, whereas the bottom panel depicts the repeated scan in the artefacted region (depicted by the arrows). The repeated scan could not remove this artefact, where the halo artefact remained visible in the same region. However, FTL-ASC successfully removed this artefact in both scans

PET-CT Fusion Based Outcome Prediction in Lung Cancer using Deep and Handcrafted Radiomics Features and Machine Learning

Arman Gorji, Ali Fathi Jouzdani, Nima Sanati, Mahdi Hosseinzadeh, Ali Mahboubisarighieh, Seyed Masoud Rezaeijo, Mehdi Maghsudi, Sara Moore, Leung Bonnie, Carlos Uribe, Cheryl Ho, Arman Rahmim and Mohammad R Salmanpour

Journal of Nuclear Medicine June 2023, 64 (supplement 1) P1196;

Tensor Deep versus Radiomics Features: Lung Cancer Outcome Prediction using Hybrid Machine Learning Systems

Mohammad R Salmanpour, Mahdi Hosseinzadeh, Nima Sanati, Ali Fathi Jouzdani, Arman Gorji, Ali Mahboubisarighieh, Mehdi Maghsudi, Seyed Masoud Rezaeijo, Sara Moore, Leung Bonnie, Carlos Uribe, Cheryl Ho and Arman Rahmim

Journal of Nuclear Medicine June 2023, 64 (supplement 1) P1174;

Advanced Survival Prediction in Head and Neck Cancer using Hybrid Machine Learning Systems and Radiomics Features

Mohammad R. Salmanpour[a,b,c*]; Mahdi Hosseinzadeh[c,d]; Ensiyeh Modiri[c,e]; Azizeh Akbari[c,f] ;Ghasem Hajianfar[c,g]; Dariush Askari[h]; Mehdi Fatan[c]; Mehdi Maghsudi[g]; Hanieh Ghaffari[c]; Seyed Masoud Rezaeijo[i]; Mohammad M. Ghaemi[c,j]; Arman Rahmim[a,b]

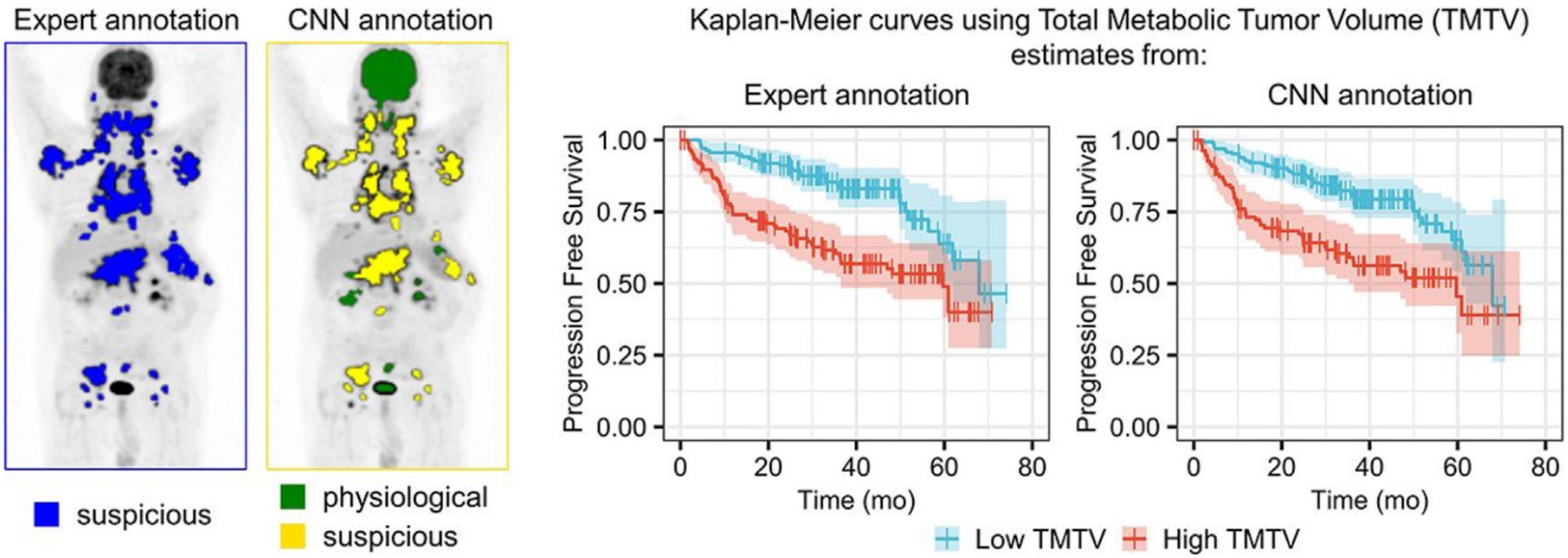

Figure 1 Stratification of progression free survival by TMTV level. This research was originally published in JNM. Capobianco et al. Deep-Learning 18F-FDG Uptake Classification Enables Total Metabolic Tumor Volume Estimation in Diffuse Large B-Cell Lymphoma. J Nucl Med. 2021 Jan;62(1):30-6.

RECIP combines **changes in total tumor volume** and **status of new lesions** and can be calculated dual-way: Visual RECIP and Quantitative RECIP.

Visual RECIP: Changes in total volume are evaluated by visual reads of nuclear medicine physicians or radiologists, and are combined with status of new lesions to calculate RECIP.

Quantitative RECIP: Changes in total tumor volume are evaluated quantitatively using tumor segmentation software and combined with status of new lesions to calculate RECIP.

Visual RECIP and Quantitative RECIP showed **95% agreement** for identifying progression vs. non-progression.

RECIP demonstrated **excellent inter-reader agreement** among 5 independent readers (complete agreement: 83% for visual RECIP and 92% for quantitative RECIP) which suggests that RECIP is ready for implementation in clinical practice.

qPSMA: Semiautomatic Software for Whole-Body Tumor Burden Assessment in Prostate Cancer Using ^{68}Ga-PSMA11 PET/CT

Andrei Gafita[1], Marie Bieth[1,2], Markus Krönke[1], Giles Tetteh[2], Fernando Navarro[2], Hui Wang[1], Elisabeth Günther[1], Bjoern Menze[2], Wolfgang A. Weber[1], and Matthias Eiber[1]

[1]Department of Nuclear Medicine, Klinikum rechts der Isar, Technical University Munich, Munich, Germany; and [2]Department of Informatics, Technical University Munich, Munich, Germany

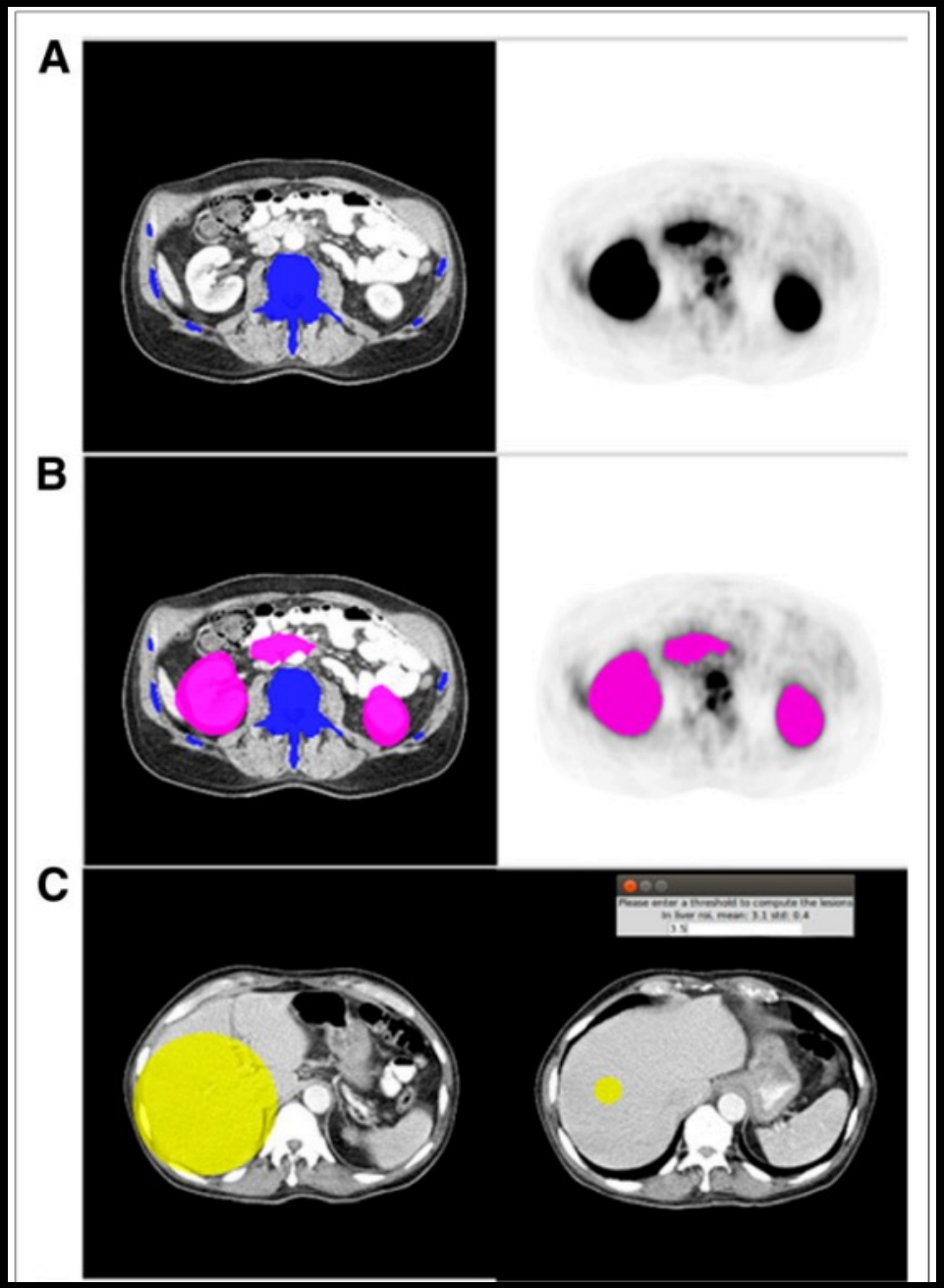

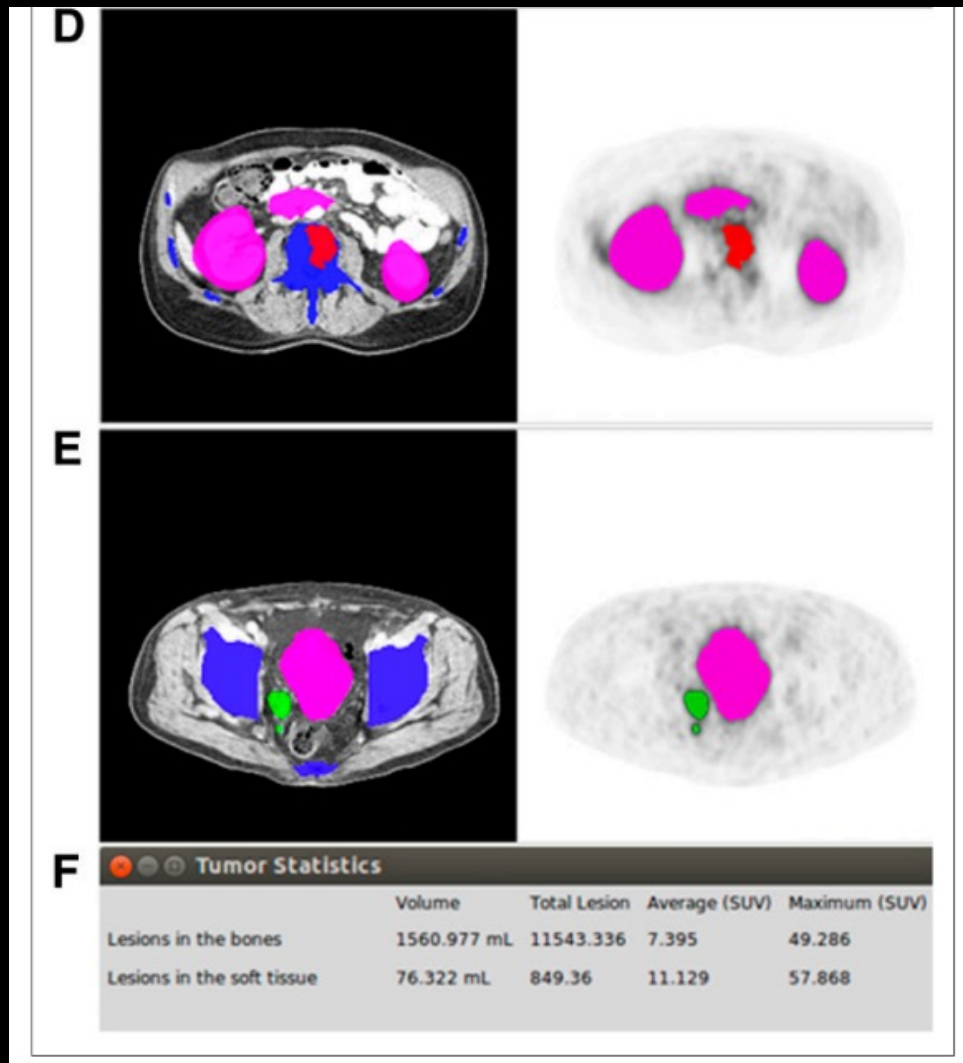

	Volume	Total Lesion	Average (SUV)	Maximum (SUV)
Lesions in the bones	1560.977 mL	11543.336	7.395	49.286
Lesions in the soft tissue	76.322 mL	849.36	11.129	57.868

FIGURE 1. The 6-step workflow of qPSMA. First, bone mask (A) and normal-uptake mask (B) are automatically computed. Then, SUV_{thr_st} is semiautomatically computed from liver background activity (C). Bone lesions are segmented using SUV_{thr_bone} (D), whereas soft-tissue lesions are segmented using SUV_{thr_st}, previously calculated at third step (E). Finally, output parameters are obtained by performing general statistics (F).

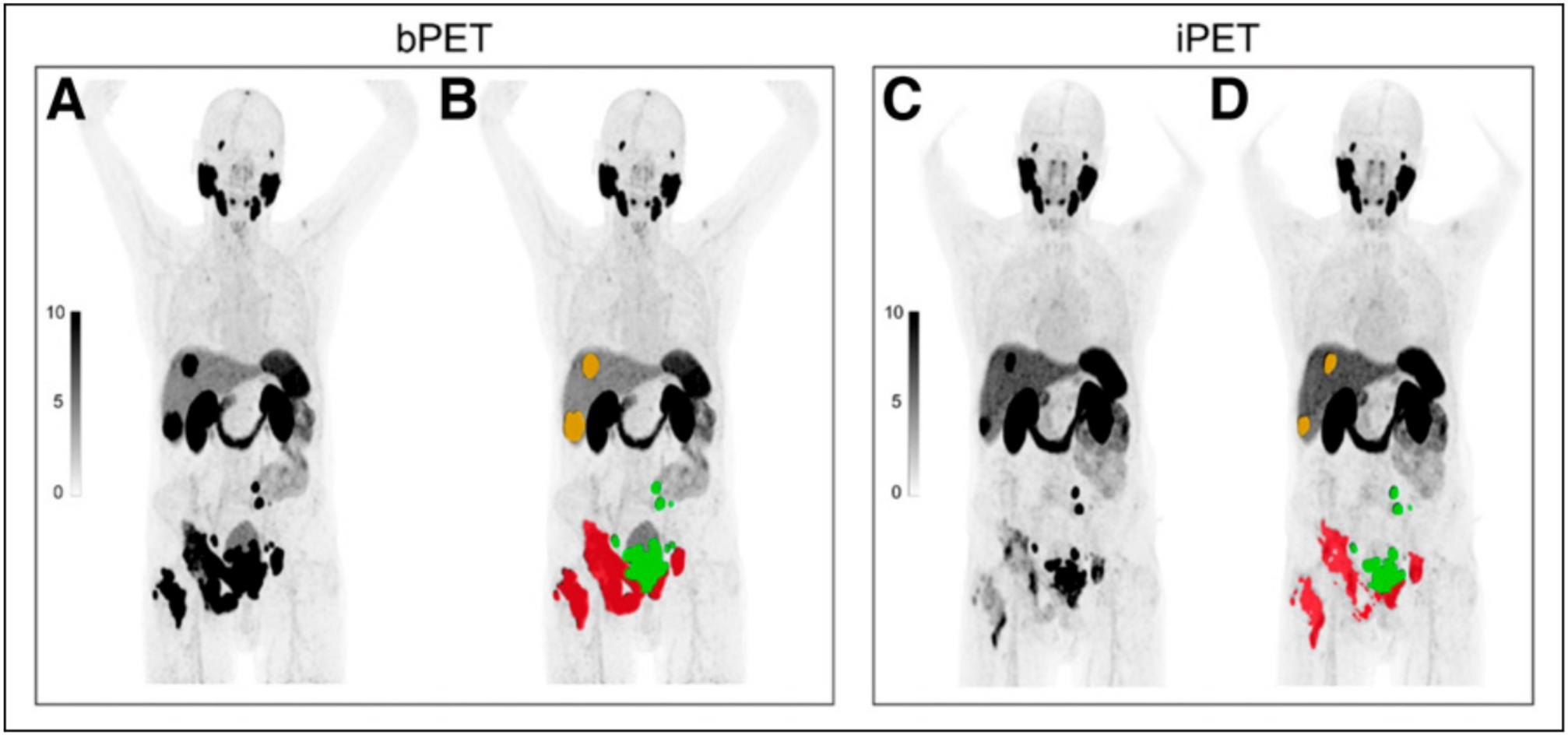

FIGURE 2. Changes in tumor burden on semiautomatic quantitative assessment of ^{68}Ga-PSMA-11 PET/CT imaging using qPSMA software. Tumor lesions on bPET and iPET ^{68}Ga-PSMA-11 PET/CT scans were segmented. Manual adjustments were performed when necessarily. Whole-body PSMA-VOL was extracted. DICOM images (A and C) are uploaded by user, and semiautomatic tumor segmentation (B and D) of bone (red), lymph node (green), and visceral (orange) metastases is obtained.

RECIP 1.0 Definition

RECIP integrates changes in total PSMA-positive tumor volume (PSMA-VOL) between baseline and follow-up scan and occurrence of new lesions.

Complete Response	**RECIP-CR**	Absense of any PSMA-update on follow-up PET scan
Partial Response	**RECIP-PR**	≥30% decrease in PSMA-VOL without appearance of new lesions
Progressive Disease	**RECIP-PD**	≥20% increase in PSMA-VOL with appearance of new lesions
Stable Disease	**RECIP-SD**	<30% decrease in PSMA-VOL with/without appearance of new lesions *or* ≥30% decrease in PSMA-VOL with appearance of new lesions *or* <20% increase in PSMA-VOL with/without appearance of new lesions *or* ≥20% increase in PSMA-VOL without appearance of new lesions

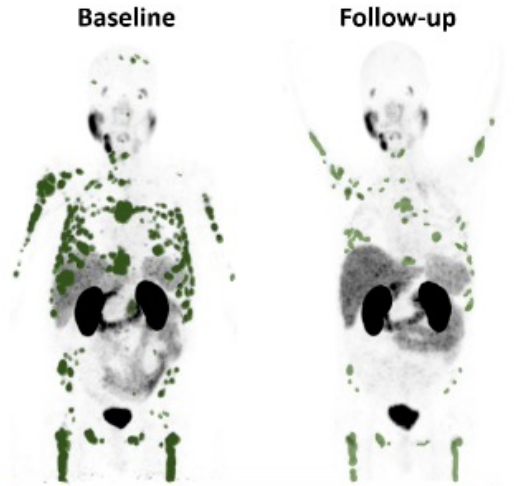

RECIP-PR
PSMA-VOL: decline ≥30%
New Lesions: -

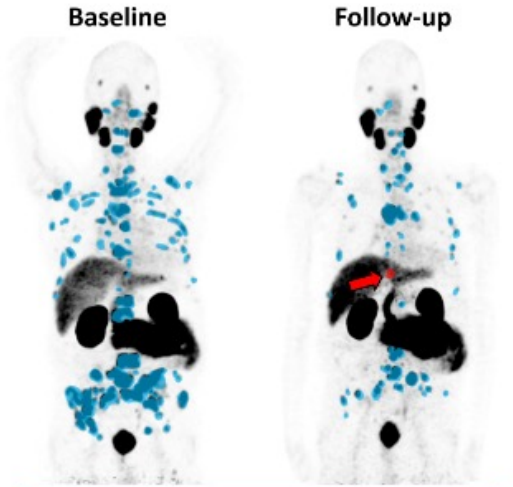

RECIP-SD
PSMA-VOL: decline ≥30%
New Lesions: +

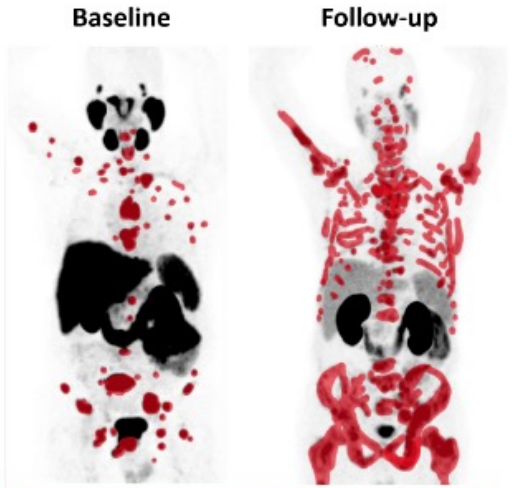

RECIP-PD
PSMA-VOL: increase ≥20%
New Lesions: +

Virtual Images

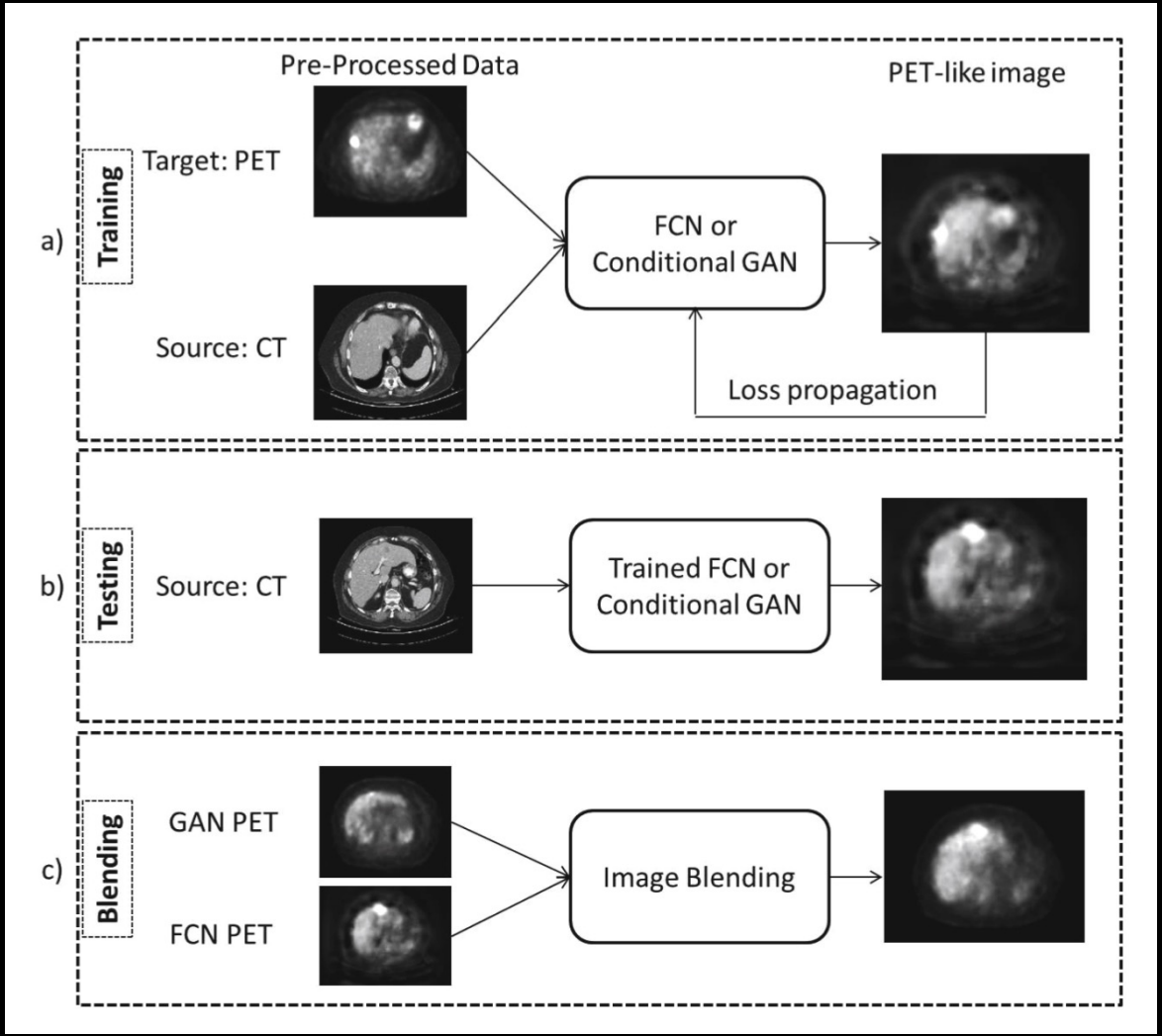

Computer Science > Computer Vision and Pattern Recognition

[Submitted on 30 Jul 2017]

Virtual PET Images from CT Data Using Deep Convolutional Networks: Initial Results

Avi Ben-Cohen, Eyal Klang, Stephen P. Raskin, Michal Marianne Amitai, Hayit Greenspan

Future of AI in NM

Future Prospects	Summary
Radiomics and Predictive Modeling	AI-driven models utilize radionics to predict disease progression, providing a comprehensive understanding of the disease's progression and enabling personalized treatment strategies.
Theranostics and Targeted Radiopharmaceuticals	AI is revolutionizing theranostics, enhancing targeted therapy and therapy planning, thereby revolutionizing radiopharmaceutical development and providing real-time adjustments.
Real-time Decision Support	As an intelligent companion, AI provides instant guidance in complex diagnostics, transforming patient care and enhancing efficiency in nuclear medicine.
Ethical Considerations	AI is revolutionizing nuclear medicine, transforming patient privacy, and ensuring transparent decision-making, requiring rigorous testing and global collaboration for responsible deployment.

Artificial Intelligence in Nuclear Medicine: Current Applications and Future Prospects

Farshid Gheisari[1], Niloufar Ebrahimi[2] and Reza Vali[3*]